onto an ~5-μm diam spot on the crystal using a 10× microscope objective, which also served to collimate the CdS fluorescence. A polarizing beam splitter separated the vertically polarized pump light from the horizontally polarized CdS emission.

Thresholds as low as 25 mW have been observed using an unmode-locked pump beam. An 8% transmitting output coupler yielded 8.8 mW out for 90-MW input power. With a prism inserted into the cavity, the laser could be tuned from 495 to 501 nm, while maintaining the 0.1-nm linewidth. In addition, when the temperature of the sample was raised from 95 to 140 K, the laser wavelength could be increased to 504 nm. Lasing could be accomplished using any of the 488-, 476-, 473-, or 458-nm lines of the Ar^+ laser as a pump.

For synchronous pumping the Ar^+ laser was actively mode-locked to produce 100-psec pulses on the 476-nm line, and the cavity was lengthened to 1.8 m. The pulse width was measured in an autocorrelator using a lithium formate crystal. Typical spots gave stable 10–12-psec (assuming a single-sided exponential shape) pulses with 3–5-mW output power and 50 mW of pump power. Up to 26 mW of output power could be maintained for a short while.

The cavity length can be changed by 500 μm without adversely affecting the pulse shape. This is in sharp contrast to synchronously pumped dye lasers, where changes of only microns can drastically alter the pulse shape. This indicates that passive pulse-shaping may be taking place. The output spectrum is much broader than that encountered in cw operation, and often lasing in more than one mode of the crystal Fabry-Perot occurs. Antireflection coating of the crystal face to eliminate these modes would increase the cavity bandwidth and possibly result in shorter pulses.

We hope this technique can be extended to other semiconductors such as AlGaAs and thus make available a picosecond pulse source easily tunable throughout the visible and near IR. **(13 min)**

1. T. C. Damen, M. A. Duguay, J. M. Wiesenfeld, J. Stone, and C. A. Burrus, in *Picosecond Phenomena II*, R. M. Hochstrasser *et al.*, Eds. (Springer, New York, 1980), p. 38.
2. E. P. Ippen, D. J. Eilenberger, and R. W. Dixon, *Picosecond Phenomena II*, R. M. Hochstrasser *et al.*, Eds. (Springer, New York, 1980), p. 21.

WR5 Picosecond switching with photoelectrons

S. WILLIAMSON, S. LETZRING, and G. MOUROU, University of Rochester, Laboratory for Laser Energetics, Rochester, N.Y. 14623.

We report on a picosecond switching technique based on electron-bombarded semiconductor and on bulk high resistivity semiconductors. The switching element is made of nearly intrinsic silicon, Cr:doped GaAs, or amorphous materials and is integrated in a microstrip or coaxial geometry. It is mounted in the image plane of a streak camera tube. A dc bias of the order of a few tens of volts is applied across the switching crystal of 500-μm thickness. The photoelectron stimulus is generated by the action of a 20-psec UV optical pulse on a gold photocathode. Previous streak camera characterization has shown that the photoelectron burst is a faithful temporal and spatial replica of the laser pulse. The photoelectrons released by the photocathode are in the 1-eV range and are accelerated to 20 keV. Each photoelectron striking the semiconductor gap implants at the surface a number of e.h. pairs $N = E/\epsilon$, where E is the photoelectron energy after amplification, and ϵ is the mean energy necessary to create an e.h. pair. In the case of silicon, ϵ is 3.6 eV, the absorption of one photoelectron leads to the creation of 6000 e.h. pairs. The photoelectron energy loss per unit length is $dE/dx = -3$ keV/μm leading to a photoelectron penetration depth of a few micrometers. The absorption of only 10^9 photoelectrons is sufficient to create throughout the gap a degenerate layer leading to efficient electrical switching. In a manner similar to photoconductive switching on an equivalent geometry, the switching time is essentially limited by the stimulus pulse width. This approach offers a number of prominent advantages over the picosecond photoconductive switching demonstrated in the past.[1]

(1) The gain in e.h. pair generation results in a decrease in the switching energy requirement of a factor of 100–1000 depending upon the quantum efficiency of the photocathode while preserving the switching rise time.

(2) The photoelectron beam can be deflected relatively easily by a rf signal[2] synchronized with the optical light burst, and different switching elements can be activated in a picosecond sequence.

(3) Any semiconductor materials can be utilized regardless of their band gap energy making possible the construction of switching devices with good voltage hold-off characteristics.[3] **(13 min)**

1. D. H. Auston, Appl. Phys. Lett. **30**, 84 (1977).
2. A. Adams, D. J. Bradley, and W. Sibett, *Picosecond Phenomena* (Springer, Heidelberg, 1978).
3. G. Mourou and W. Knox, Appl. Phys. Lett. **35**, 492 (1979).

Wednesday **AFTERNOON**

10 June 1981 **WS**

BALLROOM WEST

3:30 PM **Components and Noise in Fiber Systems**

Jan Conradi, Presider

WS1 Dispersive birefringent filters for laser communications

POCHI YEH, W. GUNNING, R. HALL, and J. TRACY, Rockwell International Science Center, Thousand Oaks, Calif. 91360.

Birefringent filters play an important role in many optical systems whenever filters of extremely narrow bandwidth with wide angular fields or with tuning capability are required. In the area of laser communication, when the signal is transmitted through a random medium, such as an atmosphere or seawater, the received signal is carried in part by a scattered component of the laser radiation which will appear to come from a wide FOV, often up to several steradians. Under these severe circumstances optical communications require a filter with not only an extremely narrow bandwidth to reject the unwanted background light and hence increase the SNR, but also a large angular aperture to receive as much signal as possible. These filters are composed of birefringent crystal plates (wave plates) and polarizers. A subangstrom birefringent filter made of materials such as quartz, calcite, and ADP requires very thick crystal plates and yet only provides a moderate FOV.

This paper investigates the properties of dispersive birefringent filters that are made of materials with a strong dispersion in birefringence. Many crystals are found to exhibit anomalous dispersion of birefringence in the spectral regimes near the absorption band edges. We will show that such a filter using CdS can provide an extremely narrow bandwidth and an enormous FOV because of the sharp dispersion and small birefringence.

The bandwidth $\Delta\lambda_{1/2}$ (FWHM) of such an N-stage Lyot filter[1,2] is given by[3,4]

$$\Delta\lambda_{1/2} = 0.886\,\frac{\lambda}{2^N|\alpha - \Delta n/\lambda|d} \sim 0.886\,\frac{\lambda}{2^N\alpha d}, \qquad (1)$$

where d is the thickness of the thinnest plate, $\Delta n = (n_e - n_o)$ is the birefringence, λ is the passband wavelength, and $\alpha = \partial\Delta n/\partial\lambda$ is the rate of dispersion of birefringence. The last equality in Eq. (1) holds for the case when $\alpha \gg \Delta n/\lambda$. The FOV of a dispersive Lyot 1 filter[2] is given by[3,4]

$$\theta = \pm n\left(\frac{2n}{\Delta r}\right)^{1/2}\left(\frac{\alpha\Delta\lambda_{1/2}}{\Delta n}\right)^{1/2}, \qquad (2)$$

where we assumed $\alpha \gg \Delta n/\lambda$.

CdS crystals exhibit a dispersion rate of $\alpha \sim 10^{-4}$ Å^{-1}. Thus a wide-field Lyot filter made of CdS crystal plates of 3.4 mm would have a bandwidth of 1 Å at $\lambda \sim 5300$ Å and a FOV of 2π ($\theta = \pi/2$). A conventional wide-field Lyot filter made of quartz with the same bandwidth would require a thickest plate of 14 cm and yet only provide a FOV of 23°.

This filter concept has been demonstrated experimentally using 2-mm thick CdS crystal plates. The measured transmission characteristics are in good agreement with our calculation. Both theory and experimental results will be presented. **(13 min)**

1. B. Lyot, Ann. Astrophys. **7**, 31 (1944); C. R. Acad. Sci. **197**, 1593 (1933).
2. J. Evans, J. Opt. Soc. Am. **39**, 229 (1949); **48**, 142 (1958).
3. P. Yeh, Opt. Commun. to be published.
4. P. Yeh and J. Tracy, Proc. Soc. Photo-Opt. Instrum. Eng. to be published.

WS2 Total switching of unpolarized light with an electrooptic liquid-crystal device

J. A. MARTIN-PEREDA and M. A. MURIEL, Ciudad Universitaria, E.T.S. Ingenieros de Telecomunicacion, Departamento de Electronica Cuantica, Madrid-3, Spain.

This paper reports a new family of multimode fiber-optic switching devices based on nematic liquid crystal devices reported by us previously. These devices have a wedged structure as the main characteristic. Several modes of behavior can arise depending on the internal configuration of the molecules. As we show, they have the possibility of total switching of unpolarized light with a very simple structure, low insertion losses, and very low operating voltages. These new devices should find a wide range of applications in fiber-optic communication systems.

The basis of this proposed switching method is the use of a wedge structure with nematic liquid crystal inside. We have used it both as a digital and analog light beam deflector. By using the same concepts these structures will yield a new concept in switching and modulating.

This device consists of two fundamental parts: a Wollaston prism (Fig. 1) and the active part of our device.

The Wollaston prism consists of two wedges, both with homogeneous configurations, the difference being the molecular directions. The first has the molecular direction perpendicular to the vertex and the second parallel to it. An unpolarized ray crossing this structure will be split into two rays. For small values of the wedge angle α, the angles of these rays with the perpendicular to the frontal surface are given by $\alpha_I \simeq \alpha_D \simeq \alpha\Delta n$, with $\Delta n = n_e - n_o$. Ray I will be polarized normal to the plane and D orthogonal to I.

These two emerging rays are now, after the

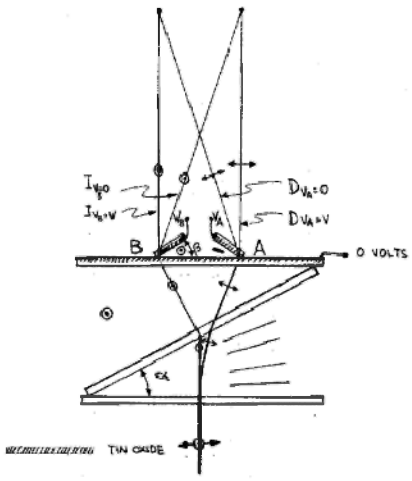

WS2 Fig. 1. Proposed switching method.

Wollaston prism, cross structures as can be seen in Fig. 1. The one labeled B has an homogeneous configuration with the direction parallel to the vertex. The other, labeled A, is perpendicular. The emerging rays adopt one of two possible directions depending on the voltage applied to the cell.

If the distance between the points where the rays emerge is properly selected, the rays will coincide at points located in a plane parallel to the common plane of the wedges. In this case, the entire radiation crossing the Wollaston prism will converge at a single point. This point is one of two possible points, depending on the voltage applied to the system.

In this paper we analyze the influence of the geometrical and electrical parameters for optimum operation. The liquid crystal to be used must have positive anisotropy. In our case we chose MBBA + PEBAB. The voltage range was between 0 and 10 V. The highest frequency we achieved has been ~20 kHz. **(13 min)**

WS3 Modal noise in multimode fibers: polarization effects

ERIC G. RAWSON, Xerox Research Center, Palo Alto, Calif. 94304; and JOSEPH W. GOODMAN, Stanford University, Department of Electrical Engineering, Stanford, Calif. 94305.

It is well known that, in certain necessary conditions, a changing speckle pattern exists at the output plane of a multimode optical fiber which can cause signal power fluctuations known as modal noise. The necessary conditions are generally stated as: (1) a sufficiently narrow source spectrum and a sufficiently short fiber length so that the coherence length of the source is greater than the fiber's modal dispersion; (2) either fiber movement or source frequency shift; and (3) spatial filtration at a fiber output plane (such as at a misaligned connector).

In this paper we show that transmission of the optical signal through a polarization-sensitive element is an effective alternative to spatial filtration in meeting the conditions for modal noise. We also show that, in the absence of spatial filtration, fiber motion does not cause modal noise directly by causing variations in the coupling to radiative modes; rather, fiber motion causes power exchange between polarizations and among different speckles; intensity variation (modal noise) only arises if this speckle pattern is spatially filtered or is passed through a polarizaton-sensitive element.

The data points in Fig. 1 show the measured signal-to-modal-noise (S/N) ratio, $\bar{I}/\sigma_I$, as a function of the area fraction ρ^2, where $\bar{I}$ is the mean, and σ. the standard deviation, of the signal, and $\rho = r/r_{core}$, where r is the radius of an aperture stop centered on the fiber core, and r_{core} is the fiber core radius. When $\rho^2 \sim 0$, it is reasonable to assume that the intensities of the visible speckle cells are independent. Since the means and variances of M independent variables add, the S/N ratio is

$$\frac{\bar{I}}{\sigma_I} = \frac{M}{\sqrt{M}} = \sqrt{M}. \tag{1}$$

The number of modes N supported by a step-index fiber is given by

$$N = 2\left[\frac{\pi r_{core}\,\text{N.A.}}{\lambda_0}\right]^2, \tag{2}$$

where N.A. is the fiber's numerical aperture, and λ_0 is the vacuum light wavelength. For the fiber used in this experiment (Galite 5000; N.A. = 0.193; core diam = 65 μm), Eq. (2) yields $N = 1930$. Since speckle in a step-index fiber is spatially invariant, the number of modes (and the number of speckles) M illuminating the detector through a stop of fractional area ρ^2 is given by

$$M = N\rho^2. \tag{3}$$

Figure 1 verifies that, when $\rho^2 \ll 1$, the measured S/N ratio is accurately predicted by Eq. (1).

As $\rho^2 \to 1$, however, the S/N ratio deviates increasingly from that predicted by Eq. (1). We show that this is because tie assumption of independence of intensities of the speckle cells is incorrect. Consider the limiting case where the total intensity on the fiber end is exactly constant; speckle scintillation then simply reflects the interchange of optical power between polarizations and between different speckle cells. Thus the modal noise present on the full fiber ($\rho^2 = 1$) is zero ($\bar{I}/\sigma_I = \infty$). Furthermore, just as when a small number of cells are visible, σ_I is proportional to the number visible, so also when a small number of cells are covered the variance σ_I^2 will be proportional to the number covered. Thus, when the fractional area $\rho^2 \sim 1$, the S/N is given by

$$\frac{\bar{I}}{\sigma_I} = \frac{M}{\sqrt{N-M}}, \tag{4}$$

where $N - M$ is the number of speckle cells masked from view. Figure 1 shows that, in the region where $\rho^2 \sim 1$, the measured S/N ratio is accurately predicted by Eq. (4).

In the absence of any polarization-sensitive component and any spatial filtration, there is little or nc modal noise. On the other hand, the inclusion of a polarization analyzer, which removes the contributions of half of the fiber modes, was found to introduce modal noise about equal to that observed when masking half of the core area (i.e., at $\rho^2 = \frac{1}{2}$). If spatial filtration is also applied, additional modes are removed, and Eq. (1) approximates the S/N ratio dependence on ρ^2 in the presence of a polarization analyzer, as was previously reported.

These observations suggest that, in the absence of spatial filtration, fiber-motion-induced modal noise does not arise principally because of changes in the coupling of power from guided to radiative modes. Instead fiber motion appears to cause random exchanges of power between polarizations and between different speckle cells; subsequently, a spatial filter or a polarization analyzer can convert these power exchanges into power fluctuations.

It can be seen in Fig. 1 that neither of the two asymptotic expressions accurately predict the measured S/N ratio in the central region ($\rho^2 \sim \frac{1}{2}$). A more detailed consideration of this case, and of the implications of this modal noise model, will be presented. **(Invited paper, 25 min)**

WS4 Interferometric measurement of temporal coherence and lime-varying longitudinal-mode wavelengths in GaAs diode lasers

PAUL MELMAN and W. JOHN CARLSEN, GTE Laboratories, Inc., Waltham, Mass. 02114.

One major source of modal noise in optical fiber communication systems originates in the rapid changes, or chirping, of the laser diode emission wavelengths as the laser junction heats and cools with the pulsed modulation of the drive current. A multimode fiber with finite differential mode delay will convert this wavelength chirping to time variations in the lateral intensity distribution, or speckle pattern, at large distances from the source, giving rise to modal noise at lossy interfaces. We have used a Michelson interferometer arrangement to analyze the chirping in a pulsed stripe-geometry diode laser, as well as quantitatively to measure the coherence length of the laser emission and the details of the wavelength variation as a function of time within the pulse.

The contrast of the interference fringes observed at the output, expressed as a function of the transit-time difference τ between the two interferometer arms, has been shown to be directly related to the second-order correlation function of the radiation. When normalized, this contrast function is equal to the coherence function.

For a multilongitudinal-mode laser, the coherence function is modulated periodically in τ, and the envelope connecting the peaks[1] is the coherence function of one of the modes if the modes are equally spaced and of the same width. If these conditions are not satisfied, as for a real laser, the envelope falls off faster[2] than the single-mode coherence function, resulting in a shorter measured coherence length. In pulsed operation of such lasers, this coherence length will be further shortened by an amount which depends on the pulse length relative to the characteristic phase fluctuations and the thermal time constant.

In this paper we report the results of quantitative measurements of pulsed laser wavelength chirping and the time constants obtained. Tuning of the interferometer path length difference to one of the coherence function peaks results in fringe pattern motion at a rate directly proportional to the rate of wavelength shift of the longitudinal modes. This configuration has the feature that the concurrent motion of the gain curve does not contribute to the observed effect. Thus only the motion of the Fabry-Perot resonances of the laser is measured.

A stripe-geometry double-heterojunction laser with a stripe 8 μm wide by 250 μm long was used. The rate of laser wavelength change as a function of lime during a pulse was determined by measuring the rate of fringe motion past a pinhole at the interferometer output. Figure 1 shows a plot of the observed variation of the chirping rate per unit dissipated power as a function of time for four different combinations of bias drive current and pulse heigh'. Two time constants are easily distinguishable, assuming the function is the sum of two exponentials, as indicated by the solid curve. The initial short time constant of 1.65 μsec can be attributed to a steady state distribution in the GaAs chip. A longer time constant of 12.6 μsec then takes over and can be attributed to the heat flow into the copper heat sink used with the laser. This rate is determined by the thermal impedance of the bond between the laser chip and the heat sink.

The calculated rate of temperature increase in the active region fits very well a function having the form of the sum of two exponentials with these two time constants for all four operating conditions. The different bias drive currents for each case determine the bias temperature and wavelength but appear to have no noticeable effect on the chirp rate. The pulse height, however, does. The rate of wavelength (and therefore temperature) increase at any given time is directly proportional to the step increase in dissipated power due to the current pulse height.

The rate of wavelength shift also determines the frequency of modal noise in fibers, where the path length difference is created by the differential mode delay rather than the unequal interferometer arms. The speckle pattern motion replaces the interferometer fringe motion. Using this analogy, one would expect a much lower modal noise frequency at short distances from the source, since the very small transit time differences will result in very small frequency differences among the modes of the fiber. At greater distances from the source, the larger modal transit time differences produce much higher beat frequencies among the modes.

We have verified this experimentally with different lengths of multimode graded-index fibers. At 1 m from the source, the modal noise was below 10 kHz, which could easily be filtered out in many digital data links, but at 50 m the modal noise spectrum extended to 250 kHz. The frequency should continue to increase with even longer fiber distances, until the differential mode delay exceeds the coherence length. This implies that lossy connectors, couplers, etc. near the laser source will not produce